THE JOURNAL OF BIOLOGICAL CHEMISTRY VOL. 285, NO. 48, pp. 37838–37846, November 26, 2010

Structural Insight into the Mechanisms of Transport across the *Salmonella enterica* Pdu Microcompartment Shell*[S]

Received for publication, July 1, 2010, and in revised form, September 19, 2010 Published, JBC Papers in Press, September 24, 2010, DOI 10.1074/jbc.M110.160580

Christopher S. Crowley[‡], Duilio Cascio[¶], Michael R. Sawaya[§¶], Jeffery S. Kopstein[¶], Thomas A. Bobik[‖], and Todd O. Yeates[‡¶1]**

*From the [‡]Molecular Biology Institute, [§]Howard Hughes Medical Institute, [¶]Department of Energy Institute for Genomics and Proteomics, and **Department of Chemistry and Biochemistry, UCLA Los Angeles, California 90095 and the [‖]Department of Biochemistry, Biophysics, and Molecular Biology, Iowa State University, Ames, Iowa 50011*

Bacterial microcompartments are a functionally diverse group of proteinaceous organelles that confine specific reaction pathways in the cell within a thin protein-based shell. The propanediol utilizing (Pdu) microcompartment contains the reactions for metabolizing 1,2-propanediol in certain enteric bacteria, including *Salmonella*. The Pdu shell is assembled from a few thousand protein subunits of several different types. Here we report the crystal structures of two key shell proteins, PduA and PduT. The crystal structures offer insights into the mechanisms of Pdu microcompartment assembly and molecular transport across the shell. PduA forms a symmetric homohexamer whose central pore appears tailored for facilitating transport of the 1,2-propanediol substrate. PduT is a novel, tandem domain shell protein that assembles as a pseudohexameric homotrimer. Its structure reveals an unexpected site for binding an [Fe-S] cluster at the center of the PduT pore. The location of a metal redox cofactor in the pore of a shell protein suggests a novel mechanism for either transferring redox equivalents across the shell or for regenerating luminal [Fe-S] clusters.

Bacterial microcompartment organelles are enclosed proteinaceous structures that encapsulate the sequential reaction steps for particular metabolic pathways (for recent reviews, see Refs. 1–3). Previous studies have elucidated several classes of microcompartment organelles, categorized according to their encapsulated enzymes. The prototypical member of these microcompartments is the carboxysome, which exists in autotrophic cyanobacteria and some chemoautotrophic bacteria. The carboxysome catalyzes inorganic carbon fixation from ribulose-1,5-bisphosphate and HCO_3^- via two sequentially acting enzymes, carbonic anhydrase and RuBisCO (for review, see Ref. 4). Microcompartment organelles that catalyze other metabolic reactions exist in heterotrophic bacteria, particularly the enteric facultative anaerobes. Functionally diverse microcompartments share a similar protein-based shell. Despite encapsulating distinct sets of enzymes in their interiors, the shells are all constructed by the assembly of proteins belonging to the same family of homologous BMC (bacterial microcompartment) proteins (Refs. 5 and 6; for review, see Ref. 3).

The enteric proteobacterium *Salmonella enterica typhimurium* forms a propanediol-utilizing (Pdu)[2] microcompartment for the initial steps in metabolizing the substrate 1,2-propanediol (5, 7–9). The Pdu microcompartments are heterogeneous in size, between 120–160 nm across, and appear polyhedral in shape with irregular facets (Fig. 1) (9). The architecture of the Pdu shell is likely similar to the carboxysome based on the similarity of the shell proteins in the two systems (5, 9, 10), although carboxysome microcompartments have been shown to form more regular icosahedral structures (11–13). The genes for the formation of the Pdu microcompartment are encoded within the ~19-kbp *pdu* operon, which codes for 21 genes whose products are all related to 1,2-propanediol metabolism (Fig. 1) (5, 8, 14). Transcriptional control of the *pdu* operon is induced by the presence of 1,2-propanediol, a byproduct of fermentation of plant cell wall carbohydrates (15, 16). Approximately 16 distinct Pdu polypeptides, some present in thousands of copies, are incorporated into a Pdu microcompartment (9, 10, 18).

The Pdu microcompartment encapsulates the initial two enzymatic steps for metabolism of 1,2-propanediol (Fig. 1) (9, 10). 1,2-Propanediol is initially converted to propionaldehyde by the B_{12}-dependent diol dehydratase enzyme. Propionaldehyde is then converted to propionyl-CoA by the coenzyme-A and NAD^+-dependent propionaldehyde dehydrogenase (14, 19). Additional enzymes in the Pdu microcompartment include an NADH-dependent cob(II/III)alamin reductase and an ATP-dependent adenosyltransferase for the activation of coenzyme B_{12} (20) and an ATP-dependent diol dehydratase reactivase, which releases deactivated B_{12} from the B_{12}-dependent diol dehydratase active site (8, 9, 21).

The Pdu microcompartment shell is believed to be formed by 8 distinct shell protein subunits, 7 of which are related to the bacterial microcompartment (BMC) class of proteins introduced above as the major constituents of diverse microcompartment organelles (Fig. 2) (8, 9, 18). Several x-ray crystal structures of BMC proteins have been elucidated revealing flat, 6-fold symmetric hexamers capable of packing in tile-like two-

* This work was supported, in whole or in part, by National Institutes of Health Grant AI081146.

[S] The on-line version of this article (available at http://www.jbc.org) contains supplemental Figs. S1–S5 and Table S1.

The atomic coordinates and structure factors (codes 3NGK and 3N79) have been deposited in the Protein Data Bank, Research Collaboratory for Structural Bioinformatics, Rutgers University, New Brunswick, NJ (http://www.rcsb.org/).

[1] To whom correspondence should be addressed: UCLA Dept. of Chemistry and Biochemistry, 611 Charles Young Dr. East, Los Angeles, CA 90095-1569. Fax: 310-206-3914; E-mail: yeates@mbi.ucla.edu.

[2] The abbreviations used are: Pdu, 1,2-propanediol utilizing; BMC, bacterial microcompartment; r.m.s.d., root mean square deviation.

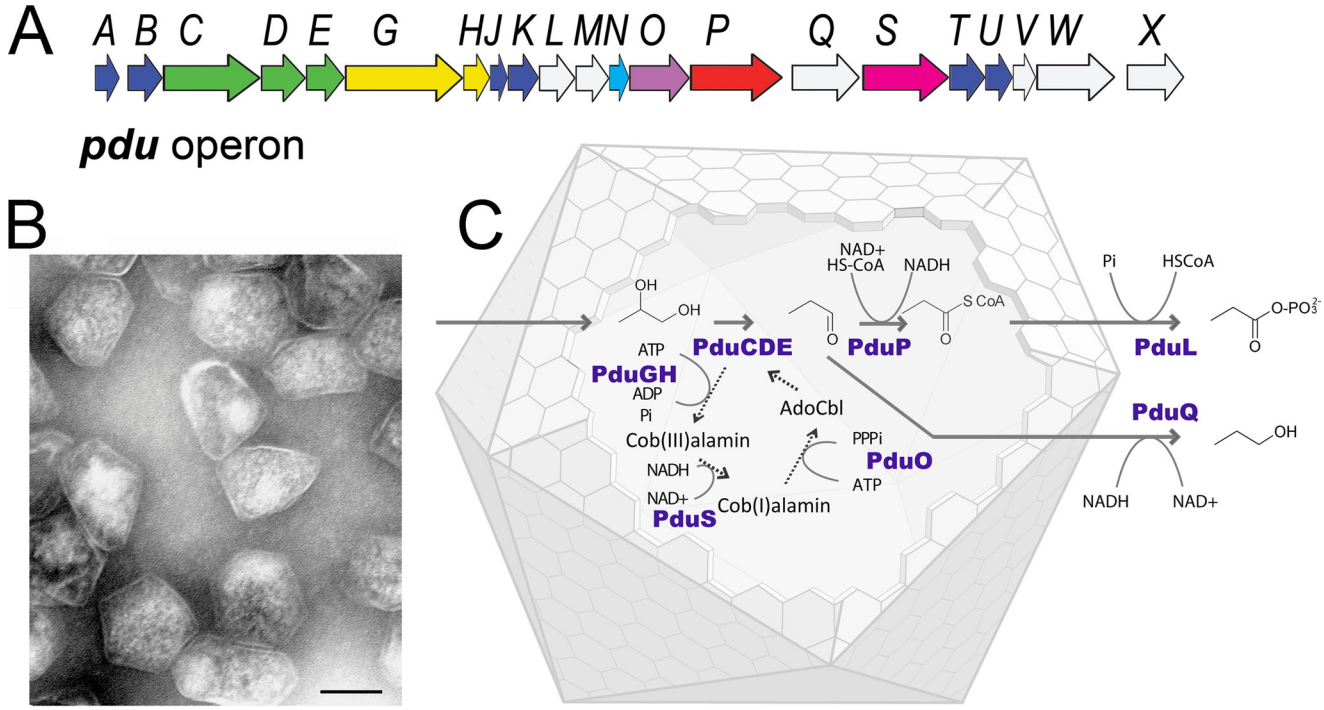

FIGURE 1. **The Pdu microcompartment.** *A*, shown is the *pdu* operon. Sixteen protein or enzyme subunits contributing to the formation of the Pdu microcompartment are encoded by genes on the 21 gene *pdu* operon, including six *pdu* BMC gene homologues (*blue*), which are predicted to form the bulk of the Pdu microcompartment shell (*pduB* gives rise to both a full-length and truncated polypeptide via alternate translation start sites, termed PduB and PduB′, respectively). *B*, shown is a transmission electron micrograph of purified Pdu microcompartments (*bar*, 100 nm). *C*, shown is a model for the structure and function of the Pdu microcompartment. The facets of the Pdu microcompartment shell are thought to be formed by the tiled packing of the BMC shell protein paralogs. The Pdu microcompartment lumen contains the enzymes for two sequential steps in the metabolism of 1,2-propanediol, carried out by the enzymes diol dehydratase (PduCDE), which is B_{12}-dependent, and propionaldehyde dehydrogenase (PduP). In addition, the Pdu microcompartment contains enzymes required to maintain the active form of the B_{12} cofactor. Adenosylcobalamin is sporadically de-adenosylated, yielding inactive B_{12} derivatives (cob(III)alamin or cob(II)alamin), which must be displaced by the diol dehydratase reactivase (PduGH). Diol dehydratase binds ADP, which is replaced during each cycle by binding and hydrolyzing an ATP molecule. The oxidized B_{12} derivatives are reduced in two successive reductive steps to the cob(I)alamin state by the bifunctional cobalamin reductase (PduS) before reactivation by the adenosyltransferase (*PduO*), yielding adenosylcobalamin. The stoichiometric balance between internal pathways that consume or generate NADH has not been determined but is presumed to favor the net formation of NADH.

```
PduA/1–94                              1 MQQE---ALGMVETKGLTAAIEAADAMVKSANVMLVGYEKIGS--GLVTVIVRGDVGAVKAAT 58
PduJ/1–91                              1 MNN----ALGLVETKGLVGAIEAADAMVKSANVQLVGYEKIGS--GLVTVMVRGDVGAVKAAV 57
EutM/1–96                              1 ME-----ALGMIETRGLVALIEASDAMVKAARVKLVGVKQIGG--GLCTAMVRGDVAACKAAT 56
CsoS1A/1–98                            1 MADVTGIALGMIETRGLVPAIEAADAMTKAAEVRLVGRQFVGG--GYVTVLVRGETGAVNAAV 61
CcmK1/1–114                            1 MSI----AVGMIETLGFPAVVEAADSMVKAARVTLVGYEKIGS--GRVTVIVRGDVSEVQASV 57
PduTD1/1–92                            1 MSQ----AIGILELTSIAKGMELGDAMLKSANVDLLVSKTICP--GKFLLMLGGDIGAIQQAI 57
PduTD2/1–92                            1 KRQ----AVGIVETWSVAACISAADRAVKGSNVTLVRVHMAFGIGGKCYMVVAGDVSDVNNAV 59
PduTD1Citrobacterfreundii/1–92         1 MSQ----AIGILELTSIAKGMEAGDAMLKSANVNLLVSKTICP--GKFLLMLGGDVGAVQQAI 57
PduTD2Citrobacterfreundii/1–92         1 KRQ----AVGIVETWSVAACICAADRAVKASNVTLVRVHMAFGIGGKCYMVVAGDVSDVNNAV 59

PduA/1–94                             59 DAGAAAAARNV-GE---VKAVHVIPRPHTDVEKILPKGISQ------------------- 94
PduJ/1–91                             58 DAGSAAASVV-GE---VKSCHVIPRPHSDVEAILPKSA--------------------- 91
EutM/1–96                             57 DAGAAAAQRI-GE---LVSVHVIPRPHGDLEEVFPIGLKGDSSN--------------- 96
CsoS1A/1–98                           62 RAGADACERV-GDG--LVAAHIIARVHSEVENILPKAPQA------------------- 98
CcmK1/1–114                           58 TAGIENIRRVNGGE---VLSNHIIARPHENLEYVLPIRYTEAVEQFREIVNPSIIRRAAA 114
PduTD1/1–92                           58 ETGTSQA----GEM---LVDSLVLANIHPSVLPAISGLNSVD------------------ 92
PduTD2/1–92                           60 TVASESA----GEKGLLVYRSVIPRPHEAMWRQMVEG--------------------- 92
PduTD1Citrobacterfreundii/1–92        58 ATGTSLA----GDM---LVDSLVLPNIHASVLPAISGLNSVD------------------ 92
PduTD2Citrobacterfreundii/1–92        60 TVASESA----GEKGLLVYRSVIPRPHESMWRQMVEG--------------------- 92
```

FIGURE 2. **Protein sequence alignment of Pdu shell proteins.** Sequences of the Pdu microcompartment shell proteins PduA, PduJ, and PduT were aligned with the shell proteins CcmK1 from the *Syn.* PCC6803 carboxysome, CsoS1A from the *Halothiobacillus neapolitanus* carboxysome, EutM from the *E. coli* K-12 Eut microcompartment, and PduT from *C. freundii*. The individual domains of the PduT proteins were aligned independently, taking residues 1–92 as domain 1 and residues 93–184 as domain 2. The conserved Cys-38 residues are *underlined* (*red line*) in both sequences. The program MUSCLE was used to perform the sequence alignment (17).

dimensional molecular layers (Ref. 11; for review, see Ref. 3). The tiled hexamer packing has been proposed to represent the *in situ* arrangement of those proteins within the context of the facets of the microcompartment shell (11, 22, 23). The structures have also revealed a mechanism by which the protein shell controls access to the lumen. The hexamers have distinct openings along their central axes that are hypothesized to serve as pores for molecular transport across the shell (11). The pores differ in their diameters and their charge properties, depending upon the residues in or around the pore openings (11, 22). Aside from the seven proteins from the BMC family, a final eighth Pdu microcompartment shell protein is homologous to the pentamer-

forming proteins, CcmL and CsoS4A, from the carboxysome, which have been proposed to occupy the vertices of that icosahedral shell (24).

The formation of the *Salmonella* Pdu microcompartment shell is required for efficient metabolism of 1,2-propanediol. The encapsulation of the first and second steps in the 1,2-propanediol pathway are necessary to limit the cytosolic exposure to propionaldehyde (10, 25, 26), produced by the first reaction step in the pathway. In *Salmonella* microcompartment shell-null mutants grown on 1,2-propanediol, the cytosolic level of propionaldehyde was elevated, leading to chromosomal mutations and cytotoxicity (26). Analogous functions (retaining a key intermediate) have been attributed to the shells of the Eut microcompartment and the carboxysome, which have been shown to restrict the diffusive loss of their respective intermediate species, acetaldehyde and CO_2 (27–29). The barrier function of the outer shell also creates a potential obstacle for the necessary movement of several relatively bulky substrates, products, and cofactors between the lumen and the cytosol. Given the current model for the Pdu microcompartment, the shell might have to allow the movement of nicotinamide cofactors, B_{12} cofactor derivatives, coenzyme-A derivatives, and phosphorylated ATP derivatives (Fig. 1). Their efficient transport could be necessary to maintain a favorable reaction environment within the microcompartment organelle and to prevent buildup of the harmful aldehyde intermediate.

Current models for molecular transport across the Pdu microcompartment shell remain incomplete. For example, the propionaldehyde dehydrogenase pathway results in a net production of NADH, which must be replaced with NAD^+ to permit continued metabolism of propionaldehyde. The exchange of oxidized and reduced NAD^+/NADH cofactors across the microcompartment shell has been suggested, but another possibility is that those cofactors are regenerated *in situ* by redox interconversions, thereby obviating their need for transport (Fig. 1) (1, 3). The maintenance of metal clusters presents another open question. The microcompartment-associated enzyme PduS contains two [Fe-S] clusters (30). If these exist on the luminal side of the shell, a mechanism for regenerating oxidatively damaged metal clusters might be required.

We present here the structure of the shell protein PduT, which reveals evidence for a role in electron or iron-sulfur cluster transport across the Pdu microcompartment shell. In addition, a structure is presented of the major shell protein PduA, whose pore structure suggests its likely role in facilitating the diffusive transport of the substrate 1,2-propanediol. Together, these structural data advance our understanding of molecular transport in bacterial microcompartments.

EXPERIMENTAL PROCEDURES

Cloning, Expression, and Protein Purification—The full-length BMC gene homologues *pduA* and *pduT* were amplified from chromosomal DNA of single *S. enterica typhimurium* colonies. *pduA* was amplified with primers to encode for a fused N-terminal Met-His_6-Gly-Thr affinity tag. *pduT* was amplified using primers to incorporate the plasmid-encoded noncleavable C-terminal Leu-Glu-His_6 affinity tag. The PCR products were ligated into the multiple cloning sites in the pET22b vector (Novagen, Darmstadt, Germany) using standard techniques. Expression plasmids for PduT C38S mutants were created by Stratagene QuikChange site-directed mutagenesis (Stratagene, La Jolla, CA) using PduT-pET22b as a template. The correctness of the resulting plasmid constructs was verified by sequencing using the dideoxy chain termination method.

PduA was expressed in selective Luria-Bertani (LB) media by 0.5 mM isopropyl β-D-1-thiogalactopyranoside induction in transformed *Escherichia coli* BL-21 (DE 3) Rosetta 2 cells (Stratagene). The protein was purified from cell lysates resulting from sonication of frozen cell pellets resuspended in 50 mM Tris and 200 mM NaCl at pH 9.0. Soluble PduA was bound to a nickel affinity column and eluted in imidazole at pH 8.0. The predominant PduA species eluted from nickel affinity was isolated by several rounds of anion exchange chromatography in Tris pH 9.0 buffer before being carried on for crystallization.

PduT and PduT-C38S proteins were expressed in transformed Rosetta 2 cells in selective LB media under 0.5 mM isopropyl β-D-1-thiogalactopyranoside induction at 30 °C. Both PduT species were isolated from sonicated cell lysates by nickel affinity chromatography. Eluted PduT C38S pET22b was further purified by anion exchange using a Sepharose Q HP column (GE Healthcare) equilibrated in Tris pH 8.0. The first eluted peak (eluting at ~250 mM NaCl), which contained relatively pure PduT in a homogeneous oligomeric state (assessed by SDS- and native-PAGE), was retained for crystallization.

Crystallography; PduA—For crystallography, PduA was concentrated to ~10 mg/ml in 30 mM Tris, pH 9.0, 50 mM NaCl, and 1% glycerol. PduA crystallization screening trials were set up using the hanging drop vapor diffusion method in 96-well Mosquito (TTP LabTech Ltd.) plates with commercially available screens from Emerald (Bainbridge Island, WA), Qiagen (La Jolla, CA), and Hampton (Laguna Beach, CA). PduA crystallized preferentially in screening conditions containing small molecular weight organic precipitants (*e.g.* ethanol, glycerol, 1-propanol, and 1,2-propanediol). Optimized PduA crystals used for diffraction had hexagonal plate morphology and formed in a condition containing 100 mM HEPES, pH 7.0, 500 mM $LiSO_4$, and 20% (v/v) 1,2-propanediol.

PduA crystals were cryoprotected for data collection in either 35% glycerol (Crystal 1) or 45% 1,2-propanediol (Crystal 2) and kept under a nitrogen stream at 100 K during diffraction. Diffraction data were collected at the Advanced Photon Source beamline 24-ID-C using a wavelength of 0.9646 Å on an ADSC Quantum 315 CCD detector (Quantum Detectors Ltd.) set at 100-mm distance. Two isomorphous crystals were used for x-ray crystal structure determination. Their space group symmetry was P622 with unit cell dimensions $a = b = 67.2$ Å and $c = 69.2$ Å. Both crystals diffracted X-rays anisotropically, with weaker diffraction along the c direction. Reflections extended out to 3.1 Å resolution for Crystal 1 and 2.3 Å for Crystal 2. Data sets were integrated, merged, and scaled using Denzo/Scalepack software (31).

Phases for diffraction intensities were obtained by molecular replacement using as a search model the structure of the homologous hexameric BMC protein EutM (Fig. 2) (PDB ID 3I6P) using PHASER (32). Subsequent rounds of refinement were carried out in PHENIX (33) and BUSTER (34). The final

model is 95% complete, containing residues 4–92 (of 94 native residues), with R_{work} = 0.25 and R_{free} = 0.28 (supplemental Table S1). The C-terminal residues that presumably form crystal contacts between layers of PduA hexamers could not be modeled, resulting in an approximate 10 Å gap between adjacent molecules within the unit cell. Aside from this missing density, we judged the structure interpretation to be reliable. The absence of non-origin peaks in a native Patterson map ruled out the possibility that the crystals were affected by a translocation disorder, as had been observed in previous BMC protein crystals (35). 94.6% of the residues were in the most favored region of a Ramachandran plot, with the remaining 5.4% of residues in the additional allowed regions. The overall quality score in the ERRAT program was 99% (36), and no major discrepancies were seen in comparison to other structures reported for this family of proteins. Structural alignments were performed using the program SUPERPOSE (32), and molecular surface area calculations were performed using the program AREAIMOL (32).

Crystallography; PduT—For crystallography, PduT C38S was concentrated to ~40 mg/ml in 25 mM Tris, pH 80, and 50 mM NaCl. Commercial screening conditions were tested by the hanging drop vapor diffusion method in a 96-well format using a Mosquito robot. PduT C38S crystallized in several screening conditions, preferentially forming three-dimensional crystals with hexagonal morphology. The best crystals were obtained in 100 mM HEPES, pH 7.0, and 1300 mM $LiSO_4$. Native crystals were immersed in Paratone-N oil (Hampton) for cryoprotection and then mounted in nylon loops under a 100 K nitrogen stream. Data were collected at the Advanced Photon Source beamline 24-ID-C at 0.9646 Å using an ADSC Quantum 315 CCD detector (Quantum Detectors) set at 125-mm distance. The PduT crystals diffracted isotropically. Native data out to 1.5 Å were integrated, merged, and scaled using the XDS data processing suite (37). PduT crystals had spacegroup symmetry $P6_3$ with unit cell dimensions $a = b = 67.7$ Å and $c = 61.6$ Å.

For heavy atom phasing, crystals were soaked in the crystallization condition plus 10 mM CsCl for 15 min and then cryoprotected in oil. The derivatized crystals remained isomorphous with the native form as judged by the absence of significant changes in unit cell parameters. Data from derivatized crystals were collected on a home source under nitrogen at 1.5416 Å using a RigakuR4++ detector (Rigaku Co.) at a distance of 100 mm. The crystals diffracted isotropically to at least 1.5 Å. Data up to 1.6 Å were used for phasing by single-wavelength anomalous dispersion from the cesium ions. An anomalous Patterson map was calculated using XPREPX (38). Three cesium ions were initially located by SHELXD (39), and a subsequent refinement step using PHASER EP identified seven additional sites (32). Phases were initially calculated to 1.6 Å using SHELXE (39), from which an initial model was built to greater than 99% completeness (residue 2–184 of 184) with R_{work} = 0.23 and R_{free} = 0.27. Native data to 1.5 Å resolution were then used to complete the model building and the atomic refinement using PHENIX (33). The final 1.5 Å resolution model includes a single PduT chain in the asymmetric unit, with R_{work} = 0.19 and R_{free} = 0.21 (supplemental Table S1). Structural alignments were performed by the program SUPERPOSE (32), and molecular surface area calculations were performed by the program AREAIMOL (32).

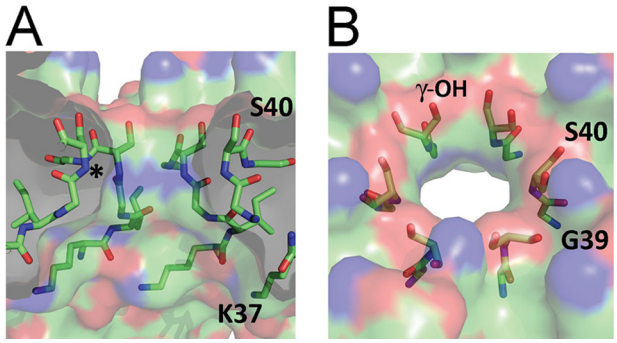

FIGURE 3. **The PduA hexamer pore.** *A*, a cut-away profile of the PduA hexamer pore shows the molecular surface. The backbone atoms of Gly-39 and Ser-40 contribute to the surface of the pore. The ring formed by six Ser-40 amide nitrogens, whose diametrically opposed atom centers are separated by 9.0 Å, form the narrowest point through the pore. The side-chain hydroxyls of Ser-40 line the opening on one side of the pore (*top of figure*), whereas the side chains of Lys-37 line the opposite side of the pore. *B*, an angled view of the PduA pore shows a stick representation of the Gly-39 and Ser-40 residues.

RESULTS

PduA—N-terminal His_6-tagged PduA protein from *S. enterica typhimurium* was expressed in *E. coli*, purified, and crystallized. The structure of PduA was determined by molecular replacement and refined at a resolution of 2.3 Å with residual errors of R_{work} = 0.25 and R_{free} = 0.29 (see supplemental Table S1 and "Experimental Procedures"). PduA forms the canonical α/β-fold first described in the BMC shell protein subunits from the *Synechocystis* PCC 6803 carboxysome shell (11). Its backbone atoms aligned with those of CcmK1 from the β-carboxysome and EutM from the Eut microcompartment with r.m.s.d. of 1.42 and 0.57 Å, respectively (supplemental Fig. S1) (23, 40). The PduA structure is most divergent from other microcompartment structures in the orientation of the C-terminal α-helix and number of C-terminal residues (residues 81–92) (supplemental Fig. S1). This site is relatively divergent between BMC paralogs and is proposed to form specific interactions with luminal microcompartment enzymes inside diverse microcompartments (23).

PduA forms a symmetric hexamer (sitting on the 6-fold axis of crystal symmetry) that is shaped like a hexagonal disc, similar to the BMC shell protein hexamers from other classes of microcompartment organelles (supplemental Fig. S1) (11, 22). The specific oligomeric packing of the PduA monomers in a hexamer is also conserved with respect to previously described classes of BMC hexamers (supplemental Fig. S1). Several hexamer structures from various microcompartment classes were overlaid on the PduA structure, giving r.m.s.d. values on backbone atoms of 0.81 Å for CsoS1A (PDB ID 3EWH) from the α carboxysome, 1.6 Å for CcmK1 (PDB ID 3BN4) from the β carboxysome, and 0.78 Å for EutM (PDB ID 3I6P) from the Eut microcompartment.

The 6-fold axis of the PduA hexamer has a patent opening through the center of the hexamer disc, which is continuous with a funnel-shaped cavity on one side of the hexamer (Fig. 3). This central patency is a defining feature of the microcompartment shell proteins and is thought to serve as a pore that selec-

tively facilitates the diffusive transport of substrates across the microcompartment shell (11). The surface within the PduA pore is mostly polar because of the exposed backbone amide N and carbonyl O atoms of Gly-39 and Ser-40, and the side-chain hydroxyl of Ser-40 near one opening of the pore. The narrowest point occurs between the symmetry-related Ser-40 backbone amide nitrogen atoms, whose atom centers are separated by 9.0 Å across the diameter of the pore, although the pore is nearly uniform in diameter over its entire length of ~10 Å. Where the pore opens into the funnel-shaped cavity on one side of the hexamer, the prominently exposed side chains of Lys-37 create a positively charged band. Based on x-ray diffraction data, an electron density feature (not attributable to PduA) is located at the center of the pore. Due to its location on the 6-fold symmetry axis, fine details of these atoms are not apparent, but the size and location suggest the possibility of a partially occupied 1,2-propanediol molecule.

The crystal structure of PduA reveals a higher order packing of the hexamers in uniform molecular sheets. The interhexamer contacts are similar to those of several other microcompartment structures, including CcmK1, CcmK2, CsoS1A, and CsoS1C; these interactions are thought to approximate the hexamer interactions in the context of the microcompartment shell (11, 22, 23, 35). The hexamers in these various structures show some variation in the spacing between neighboring hexamers, ranging between 66.4 and 70.0 Å. The closest hexamer spacing occurs in the structure of CsoS1A (66.4 Å), in which the edges between neighboring hexamers form extensive interactions (Fig. 4) (22). Analogous edge-edge interactions exist in the PduA structure, which is packed nearly as closely, with a spacing of 67.2 Å. The Lys-25 side-chain amino group hydrogen bonds with the backbone carbonyl O of the same, symmetry-related residue; the side-chain guanidinium group of Arg-79 hydrogen bonds with the backbone carbonyl oxygen atom of residue 24 (Fig. 4). The bonding interactions between hexamers in CsoS1A were proposed to facilitate their particularly close interaction. A comparison of the hexamer packing between PduA and CsoS1A by superpositioning adjacent hexamers showed slightly closer alignment between the edges of CsoS1A hexamers, however (Fig. 4). The PduA hexamer-hexamer interaction buries ~1230 Å^2 along each edge, below the typical threshold for dimeric biological interactions (~1700 Å^2) (41). However, given the relatively narrow surface strip presented at the hexamer edges and the fact that each hexamer forms contacts with six other hexamers, it is likely this interaction is a close approximation to the shell protein hexamer contacts *in situ*. The likelihood of its biological relevance is also supported by multiple observations of similar hexamer interactions in several BMC structures from diverse microcompartment classes (3).

PduT—Purified wild type PduT pET22b protein ran at the expected molecular mass on a reducing SDS-PAGE gel. Several lower molecular weight species were also present in the sample; these persisted even with protease inhibitors and subsequent rounds of anion exchange and size-exclusion chromatography (data not shown). We hypothesized that the lower-weight bands might be proteolyzed PduT fragments caused by reactive oxygen species generated at a putative PduT metal center. A

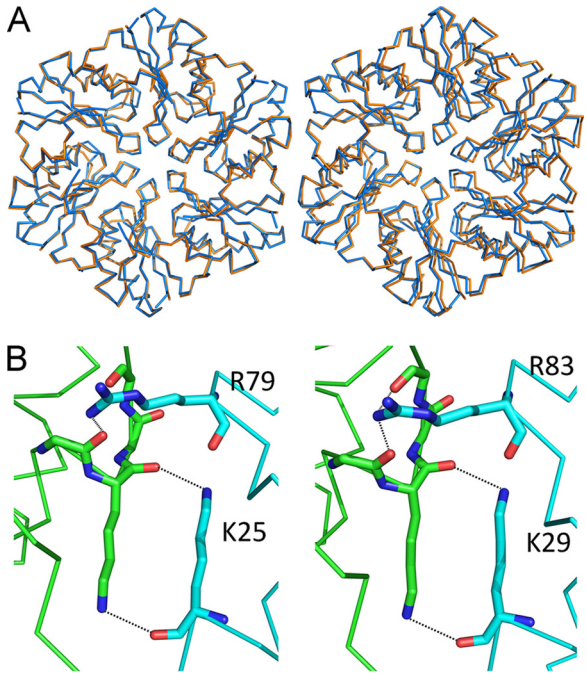

FIGURE 4. **PduA hexamer packing.** The crystal lattice layer packing of PduA hexamers (*orange ribbons*) is compared with the packing of adjacent CsoS1A hexamers from the *H. neapolitanus* carboxysome (*blue ribbons*). PduA and CsoS1A hexamers were aligned (*left*) to illustrate similarities in the packing position of each adjacent hexamer (shown on the *right*). Adjacent CsoS1A hexamer centers are separated by 66.4 Å, and contacts between adjacent hexamer edges bury substantial surface area, indicating the likely biological relevance of this hexamer packing arrangement. Likewise, the PduA hexamer centers are separated by 67.2 Å, and a substantial portion of surface area is buried along the hexamer edges. *B*, conserved interactions at the 2-fold hexamer interface of PduA (*left*) and CsoS1A (*right*) are shown. The chains from 2-fold-related hexamers are colored *cyan* and *green*. Key residues are *highlighted*.

PduT orthologue from *Citrobacter freundii* was recently shown to incorporate a [4Fe-4S] cluster via ligands contributed by residue Cys-38 (Fig. 2) (42); mutagenesis of its two other cysteines (positions 108 and 136) failed to disrupt metal binding. To eliminate the protein degradation that we hypothesized to be promoted by the metal cluster, we made a point mutation from cysteine to serine in the expression construct of the *Salmonella pduT* gene at the sequence-aligned cysteine (residue 38) (Fig. 2). *Salmonella* PduT C38S was expressed and purified in the same manner as wild type PduT and remained stable at 4 °C (data not shown). Native-PAGE analysis of nickel affinity-purified protein showed a single dominant oligomeric form with some higher-order species. The major form was enriched to near purity by anion exchange and carried on for crystallography studies. Crystals of PduT C38S diffracted strongly to 1.5 Å resolution The structure was determined using anomalous scattering from a CsCl-soaked crystal for phasing and refined with residual errors of R_{work} = 0.19 and R_{free} = 0.21 (see supplemental Table S1 and "Experimental Procedures").

PduT is a 184-residue-long member of the BMC family of proteins. The general structural features of PduT conform to the function of this class of proteins as hexagonal shell-forming subunits and as selective transport proteins for reactants into and out of the microcompartment organelles (Fig. 5). However, the structure of PduT represents a novel fold variation for the highly adaptable BMC proteins. Several fold and domain vari-

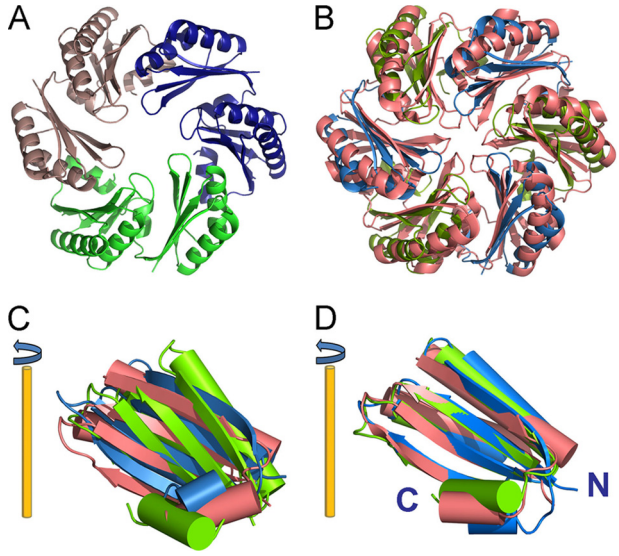

FIGURE 5. **The structure of PduT.** *A*, shown is the 3-fold symmetric, pseudohexameric PduT trimer (colored by protein chain). The individual BMC domains of PduT adopt analogous packing orientations to the six BMC domains of single-domain BMC hexamers. *B*, the packing orientations of both domain 1 and domain 2 are rotated with respect to the orientations of BMC domains in other structures. For reference, the EutM hexamer (*magenta*) is superpositioned over the PduT trimer (domain 1, *blue*; domain 2, *green*). *C*, differences between the oligomeric packing of the domains of PduT and EutM are apparent when overlaid. For comparative analysis, a 6-fold rotational symmetry operator was applied to the individual PduT domains to generate hypothetical domain 1 and domain 2 "hexamers," which were then aligned with the EutM hexamer. The PduT domain orientations, particularly for domain 2, are generally rotated away from the central axis of symmetry, creating a relatively wide central pore. The approximate position of the pore axis is drawn (*yellow*). *D*, shown is backbone superposition of the PduT domains over the canonical single domain protein EutM (domain 1, *blue*; domain 2, *green*, EutM, *magenta*). The relative position of the pore loops and the C-terminal α helices differ between domain 1 and domain 2. The approximate position of the pore is drawn in *yellow*.

ations have already been characterized in x-ray crystal structures (for review, see Ref. 3). Although six previous homologues have been of the single-domain type with the canonical fold (11, 22, 23, 40, 35), two others have been of the single-domain type but with a circularly permuted fold (40, 43), whereas four others have been two-domain tandem fusions with each domain being of the permuted variety (40, 44–46). Instead, the PduT structure forms tandem domains of the canonical (*i.e.* non-permuted) variety of the α/β BMC fold, connected by a short linker sequence. Residues 1–88 form domain 1, and residues 94–184 form domain 2. Three PduT monomers assemble to make a 3-fold-symmetric homotrimer (situated on the 3-fold axis of symmetry in the crystal) structurally similar to the typical BMC homohexamers (Fig. 5). The domain packing of the tandem PduT domains is nearly analogous to that of single BMC domains within the canonical BMC hexamer structures. The distinctive 3-fold symmetric packing of BMC domains, however, ideally suits the structure of PduT for binding a metal cluster at its central pore.

The tandem domains within PduT have divergent sequences, but their structures both conform closely to the canonical BMC fold. The individual PduT domain sequences are only 24% identical to each other (Fig. 2). The sequence identity between the individual domains of the four previously solved tandem-BMC structures are comparably low (all are below 21%) (40, 44–46). However, the PduT domain structures align closely, similar to the domains of other tandem BMC proteins; domain 1 Cα 3–72 were aligned with domain 2 Cα 95–168 with a r.m.s.d. = 1.14 (Fig. 5). The PduT domain folds were also aligned with the canonical BMC structure of EutM from the evolutionarily related Eut microcompartment (40); domain 1 residues 2–75 aligned with a r.m.s.d. = 1.45; domain 2 residues 95–177 aligned with a r.m.s.d. = 1.26 (Fig. 5). The most significant structural differences between the PduT domains occur at the loop positions lining the pore and at their C termini. The domain 1 loop (residues 37–41) has two fewer residues than the domain 2 loop (residues 128–135) and forms a tighter turn. The alternate conformations of the C-terminal helices result from the distinct BMC domain packing arrangement of the PduT trimer.

PduT forms a 3-fold-symmetric trimer with flat, hexagonal-shaped disc morphology. Rather than the pseudo-6-fold symmetrical BMC domain packing observed in previously determined tandem-domain BMC protein structures, the symmetrical packing of BMC domains in the PduT trimer is broken (Fig. 5) (40, 44–46). With respect to domain 1, the orientation of domain 2 is rotated out of the plane of the trimer and away from the central 3-fold axis. This rotated orientation creates a distinctly triangular opening at the central pore (Fig. 5). The skewed packing of domain 2 appears to correlate with a major conformational change in the C-terminal α-helix. In domain 2, the axis of this helix is directed away from the central pore so that one side of the helix contributes several residues to the surface of the central pore. By comparison, the axis of the analogous helix of domain 1 is directed toward the central pore, and only the residues at its C terminus are solvent-exposed.

The PduT C38S pseudohexamer pore is the apparent binding site for a [4Fe-4S] metal cluster, which was detected by EPR spectroscopy in the PduT homologue from *C. freundii* (42). The ligands of the *C. freundii* metal cluster were identified in that study to be the Cys-38 side chains, and a PduT tetramer was proposed to contribute the ligands to the metal cluster. The analogous sequence position in the *Salmonella* homologue is also residue 38 (mutated from cysteine to serine here), which falls in a consensus sequence ICPG from residues 37–40 that is strongly conserved in an alignment of PduT homologues (supplemental Fig. S2). Contrary to the tetrameric arrangement proposed earlier, we show that three cysteines, one from each subunit of the trimer, line the central pore (Fig. 6). Cysteine 38 (or its serine surrogate) is situated on the conserved loop at the centermost position with respect to the pore, and its side chain extends in toward the center. The loop forms a sharp hairpin turn at the next sequence position, Pro-39, and as a result of this abrupt turn the cysteine (or serine) side chain is distinctly exposed within the pore. The 3-fold-related Ser-38 side-chain hydroxyls are separated by 8 Å; similar distances would be expected to separate the cysteine sulfur atoms that constitute the ligands to typical [4Fe-4S] sites. The pore loops of domain 2, including residues 128–135, are bent away from the pore and contribute minimal steric bulk in the vicinity of the metal binding site, with the exception of the side chains of Phe-130. The Phe-130 side chains are positioned proximal to the metal binding site with their aromatic plane normals turned nearly parallel

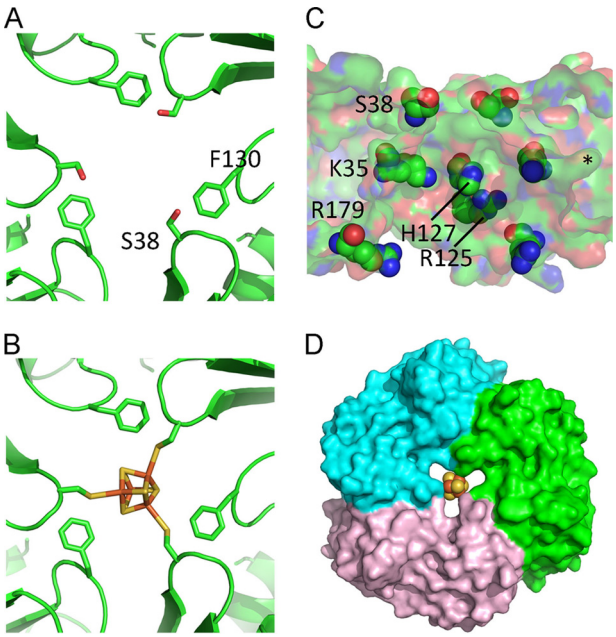

FIGURE 6. **A model for the [4Fe-4S] cluster in the PduT pore.** *A*, shown is the PduT trimer pore and its putative metal binding site, viewed along the central 3-fold axis. Ser-38, which was mutated from the wild type cysteine, occupies a loop position lining the pore, and its side chain is oriented toward the central pore axis. The symmetry-related serine hydroxyls of Ser-38 side chains are separated by ~8 Å. Phenylalanine side chains also line the pore from the analogous loop position of domain 2. *B*, shown is a modeled conformation of a putative [4Fe-4S] cluster (from ferredoxin) using cysteine substitutions for Ser-38. The cysteine side chains were modeled in alternate rotamer conformations to achieve the best fit. *C*, a side view (cut-away) of the central pore shows the molecular surface, colored by atom type. A prominent charged patch is formed by the exposed side chains of Lys-35 and Arg-125, which line a hydrophobic pocket (marked with an *asterisk*). *D*, the PduT trimer is shown modeled with a [4Fe-4S] cluster (*spheres*) at the pore opening, and the three subunits colored separately.

to the 3-fold pore axis, restricting the diameter of the pore. Several of the domain 2 loop sequence positions are also conserved in PduT homologues, including Gly-131, Ile-132, Gly-133, Gly-134, and Lys-135. The residue types aligned with position 130 are predominantly aromatic or hydrophobic amino acids (supplemental Fig. S2).

The funnel-shaped central cavity on one side of the PduT trimer bears a net positive charge and a prominent hydrophobic groove (Fig. 6). It is likely that the charged positions and the hydrophobic pocket constitute an interaction site, but no substrates were apparent during protein isolation or from the electron density. Each chain contributes three proximally situated basic side chains (Lys-35, Arg-125, and His-127) that form three distinct basic foci within the cavity near the pore plus three additional charged sites due to the exposed side chains of Arg-179 near the opening of the cavity. At a pore-proximal site, the Arg-125 Nη1 atom and His-127 Nδ1 atom are separated by 3.5 Å, and the Lys-35 Nζ and Arg-125 Nϵ atoms are separated by 7 Å. A prominent hydrophobic pocket exists at the surface position between the Lys-35 and His-127 chains, marking the beginning of a groove that extends along the surface to the metal binding site. The residues constituting this charged patch are generally conserved in PduT homologues (supplemental Fig. S2); lysine or arginine occurs at position 35, arginine or histidine occurs at position 127, and arginine 125 occurs in many PduT homologues.

Although the arrangement of the BMC domains is not strictly 6-fold symmetric, the edges of PduT trimers are nearly hexagonal in shape and formed closely packed two-dimensional molecular sheets with a lattice spacing of 67.8 Å between neighboring trimer centers. As noted above, the close-packing of trimers (or hexamers, in the case of single domain BMC proteins) with lattice spacing in the range of 66.4–70.0 Å are common in BMC protein structures (3, 40, 45). The PduT hexamer edges bury a total surface area of 900 Å^2. A small break in the otherwise continuous packing is apparent at the crystallographic 3-fold axis where three copies of PduT domain 2 come together (supplemental Fig. S3). This defect is unique to the PduT structure due to the skewed BMC domain 2 orientations, which creates a rounded hexamer corner with imperfect hexagonal tiling.

DISCUSSION

The crystal structure of the microcompartment shell protein PduA suggests it likely functions as a shell protein transporter for 1,2-propanediol, the initial substrate for the Pdu microcompartment reactions (9). This transport function is consistent with the high relative abundance of PduA observed in isolated Pdu microcompartments (9, 10). Based on the structure of the 6-fold symmetric pore, a tentative mechanism for selective transport of 1,2-propanediol can be proposed. The exposed atoms forming the pore present numerous hydrogen bond donors and acceptors. The limited resolution and high symmetry did not permit modeling water molecules or 1,2-propanediol within the pore, but hydrogen bonds from the backbone of the protein loops lining the pore to water molecules and 1,2-propanediol hydroxyl groups are likely. A similar pore might be formed by PduJ, another Pdu microcompartment BMC shell protein whose structure has not yet been determined but whose sequence is 86% identical to PduA with perfect identity over the pore-lining residues (Fig. 2) (residues 37–40). It has been proposed previously that the Pdu microcompartment shell is permeable to 1,2-propanediol, the initial substrate of the microcompartment reactions, whereas it sequesters propionaldehyde, the toxic intermediate (26). The properties of the PduA (and PduJ) pore could favor transport of the relatively hydrophilic 1,2-propanediol over the less polar propionaldehyde. Propionaldehyde presents only a single hydrogen bond acceptor and no donors, potentially limiting the speed of its efflux from the microcompartment. Alternatively, a high concentration of enzymes in a favorable arrangement inside the microcompartment might obviate the need for a selective barrier against efflux of the intermediate.

The PduA hexamer sheet is likely a close representation of the hexamer packing within the microcompartment shell. Adjacent PduA hexamers interact closely and recapitulate some of the specific atomic interactions that were hypothesized to facilitate the close-packing interaction between the CsoS1A BMC hexamers of the carboxysome shell (Fig. 4) (22). Compared with the CsoS1A structure, the PduA hexamers are slightly more widely spaced, possibly due in part to slight size differences of their hexamers. Despite the wider spacing, however, the edges between the PduA hexamers form a continuous surface without any patencies, similar to CsoS1A.

The PduT trimer also formed closely packed molecular sheets in the crystal lattice, similar to PduA (supplemental Fig. S3). The lattice spacing of PduT hexamers is close to that observed for PduA, but the interacting hexamer edges bury only about half as much area. By simple inspection of the 2-fold hexamer interface, it is not clear whether closer packing between PduT hexamers could be achieved. This is consistent with the observation that PduT is a minor component of the microcompartment shell and so must form heterologous interactions with other BMC paralogs *in situ* (9). Varying degrees of preference for non-self hexamer interactions might serve as a mechanism to direct the assembly of the heterogeneous microcompartment shells. To date, no crystal structures have been obtained to illuminate the interactions between distinct BMC paralogs that must occur in natural shells.

The quaternary structure of the PduT trimer breaks from the approximate 6-fold-symmetric packing observed in most shell protein structures, including previously characterized tandem domain BMC proteins. The novel conformation of PduT carries potential functional implications for its role in molecular transport across the microcompartment shell. Within the PduT trimer, alternate BMC domains around the oligomer are rotated away from the central 3-fold axis to accommodate a metal cluster at the pore (Fig. 6). The rotated domain packing could also accommodate the binding of a bulky substrate molecule within the pore cavity.

A *Citrobacter* PduT homologue was previously shown to incorporate a [4Fe-4S] cluster via ligands at its Cys-38 residues (42), whose analogous sequence positions we now visualize at the 3-fold pore in the structure of PduT C38S from *Salmonella*. To test the viability of binding in the *Salmonella* PduT, modeling was performed to fit a [4Fe-4S] cluster (extracted from the known structure of ferredoxin (PDB ID 1FRX)) into a cysteine-substituted PduT structure (Fig. 6). The best fit required the substituted Cys-38 side chains to adopt alternate rotamer conformations, with the sulfur atoms oriented more centrally to the pore. Allowing only this rotameric adjustment, the sulfur atoms are brought within a distance of 3.0 Å to the iron atoms. Ideal distances for those bonds are close to 2.3 Å, implying that additional minor conformational differences in the protein must be present in the wild type metal-bound configuration. The domain-1 pore loop backbone is somewhat flexible, as suggested by the relatively weak electron density over these residue positions.

A [4Fe-4S] cluster has an essentially cubic structure, and the modeled placement of the cluster orients it with its cubic body diagonal along the 3-fold axis of symmetry down the center of the pore in the PduT trimer. The metal cluster and its three cysteine ligands obey this symmetry. In addition, the [4Fe-4S] cluster calls for a fourth ligand to an iron atom lying on the 3-fold symmetry axis but displaced vertically from the other three ligands. Depending on the up *versus* down orientation of the cluster (which is not addressed by our structural data or the modeling exercise), that fourth iron atom could be situated to bind a ligand on the luminal side of the shell or the cytosolic side. The identity of the fourth ligand is not apparent from the structure. As discussed, the rotated domain orientations in PduT, compared with typical BMC hexamers such as PduA, create added space for accessing the pore. The ligand position pointing toward the presumptive cytosolic side would be especially accessible and available to bind a range of potential ligands, including proteins. Given its accessibility from both sides of the hexamer, the metal cluster in PduT is well suited for electron transport between the microcompartment lumen and the bacterial cytosol.

In addition to the metal binding site, other features of the PduT structure suggest a potential role in facilitating redox chemistry. The core of domain 2 has a potential reversible disulfide bond that might be capable of coupling redox changes to protein structural transitions that would affect the properties of the microcompartment shell (supplemental Fig. S4). In the crystal structure of PduT, Cys-108 and Cys-136 in domain 2 are positioned nearly close enough to form a disulfide bond, but their side chains adopt alternate rotamer conformations that preclude a disulfide bond (although reducing compounds were not introduced during protein purification). The formation of this disulfide bond might alter the conformation of PduT, resulting in a redox-sensitive change in its pore function. These cysteine positions are conserved in a sequence alignment of PduT homologues (supplemental Fig. S2), which is notable given the absence of disulfide bonds in the structures of other BMC shell proteins and the general absence of cysteines in most other BMC paralogs. Recently, the structure of a redox-sensitive carbonic anhydrase in the β-carboxysome was reported, suggesting the redox state of that microcompartment is regulated (47). Redox regulation could also be important in the Pdu microcompartment. Oxidizing conditions would favor the conversion of propionaldehyde to propionyl-CoA, yielding a net of one ATP, one reducing equivalent, and methylcitrate cycle intermediates. In contrast, the alternate reductive pathway for disposing of propionaldehyde expends an NADH and leads to the production and subsequent loss of 1-propanol, which is not metabolized (for review, see Ref1). Until now, mechanisms for controlling the redox environment within the Pdu microcompartment have not been evident. The observations of a potential disulfide bond and an [Fe-S] cluster at the center of the PduT trimer pore provide important clues.

Given the current model of the Pdu microcompartment reactions, PduT might facilitate the regeneration of encapsulated redox cofactors by transferring electrons across the shell. Potential mechanisms for maintaining favorable redox conditions in the lumen of the Pdu microcompartment have not been articulated, but NADH produced in the propionaldehyde dehydrogenase reaction must be regenerated to NAD^+ to permit continued oxidation of the propionaldehyde intermediate. If PduT were to facilitate oxidation of the NADH cofactor within the microcompartment, it would circumvent the need to exchange relatively bulky NAD^+/NADH molecules across the microcompartment shell. This possibility would be complicated, however, by the need for a flavin as an intermediary; [Fe-S] clusters typically accept single electrons, whereas the flavin cofactor can undergo two successive, single-electron transfers.

As an alternative to facilitating electron transport, PduT could serve to transport intact [4Fe-4S] clusters into the microcompartment. This speculative idea is based on the likely

requirement for [4Fe-4S] clusters within the Pdu microcompartment lumen. The microcompartment-associated cob(II/III)alamin reductase (PduS) has two putative [4Fe-4S] clusters per chain (9, 30, 48). Likewise, the PduK shell protein contains an extra domain C-terminal to the typical BMC domain that bears an amino acid sequence motif for binding an [Fe-S] cluster; characterization of the presumptive metal binding domain of PduK is incomplete (supplemental Fig. S5), and whether that domain is situated toward the lumen is unknown. The potential presence of [Fe-S]-containing proteins (*i.e.* PduS and PduK) on the luminal side of the shell supports the possibility that the PduT pore might be used to transport [4Fe-4S] clusters to help replace depleted clusters in those proteins. Indeed, the solvent-accessible positioning and presence of three metal ligands in PduT rather than the typical four ligands is reminiscent of [Fe-S] scaffold proteins, which only transiently bind their prosthetic groups (for review, see Ref. 49). In summary, the unexpected finding that PduT binds an [Fe-S] cluster in a pore that opens into the microcompartment lumen provides a key insight, but pinpointing the specific function of the cluster will require further studies.

Acknowledgments—We thank members of the laboratory of Professor Joan Valentine (UCLA) for technical assistance, especially Dr. Armando Durazo for help with ICP-MS. We are also appreciative of the assistance by the staff at the Advanced Photon Source Beamline 24-ID-C. We are indebted to Dr. Janneke Balk for useful discussions and the suggestion of [Fe-S] cluster transport.

REFERENCES

1. Cheng, S., Liu, Y., Crowley, C. S., Yeates, T. O., and Bobik, T. A. (2008) *BioEssays* **30,** 1084–1095
2. Yeates, T. O., Kerfeld, C. A., Heinhorst, S., Cannon, G. C., and Shively, J. M. (2008) *Nat. Rev. Microbiol.* **6,** 681–691
3. Yeates, T. O., Crowley, C. S., and Tanaka, S. (2010) *Annu. Rev. Biophys.* **39,** 185–205
4. Badger, M. R., and Price, G. D. (2003) *J. Exp. Bot.* **54,** 609–622
5. Chen, P., Andersson, D. I., and Roth, J. R. (1994) *J. Bacteriol.* **176,** 5474–5482
6. English, R. S., Lorbach, S. C., Qin, X., and Shively, J. M. (1994) *Mol. Microbiol.* **12,** 647–654
7. Shively, J., Bradburne, C., Aldrich, H., Bobik, T., Mehlman, J., Jin, S., and Baker, S. (1998) *Can. J. Bot.* **76,** 906–916
8. Bobik, T. A., Havemann, G. D., Busch, R. J., Williams, D. S., and Aldrich, H. C. (1999) *J. Bacteriol.* **181,** 5967–5975
9. Havemann, G. D., and Bobik, T. A. (2003) *J. Bacteriol.* **185,** 5086–5095
10. Havemann, G. D., Sampson, E. M., and Bobik, T. A. (2002) *J. Bacteriol.* **184,** 1253–1261
11. Kerfeld, C. A., Sawaya, M. R., Tanaka, S., Nguyen, C. V., Phillips, M., Beeby, M., and Yeates, T. O. (2005) *Science* **309,** 936–938
12. Schmid, M. F., Paredes, A. M., Khant, H. A., Soyer, F., Aldrich, H. C., Chiu, W., and Shively, J. M. (2006) *J. Mol. Biol.* **364,** 526–535
13. Iancu, C. V., Ding, H. J., Morris, D. M., Dias, D. P., Gonzales, A. D., Martino, A., and Jensen, G. J. (2007) *J. Mol. Biol.* **372,** 764–773
14. Bobik, T. A., Xu, Y., Jeter, R. M., Otto, K. E., and Roth, J. R. (1997) *J. Bacteriol.* **179,** 6633–6639
15. Bobik, T. A., Ailion, M., and Roth, J. R. (1992) *J. Bacteriol.* **174,** 2253–2266
16. Rondon, M. R., and Escalante-Semerena, J. C. (1992) *J. Bacteriol.* **174,** 2267–2272
17. Edgar, R. C. (2004) *Nucleic Acids Res.* **32,** 1792–1797
18. Parsons, J. B., Frank, S., Bhella, D., Liang, M., Prentice, M. B., Mulvihill, D. P., and Warren, M. J. (2010) *Mol. Cell* **38,** 305–315
19. Leal, N. A., Havemann, G. D., and Bobik, T. A. (2003) *Arch. Microbiol.* **180,** 353–361
20. Johnson, C. L., Pechonick, E., Park, S. D., Havemann, G. D., Leal, N. A., and Bobik, T. A. (2001) *J. Bacteriol.* **183,** 1577–1584
21. Mori, K., Tobimatsu, T., Hara, T., and Toraya, T. (1997) *J. Biol. Chem.* **272,** 32034–32041
22. Tsai, Y., Sawaya, M. R., Cannon, G. C., Cai, F., Williams, E. B., Heinhorst, S., Kerfeld, C. A., and Yeates, T. O. (2007) *PLoS Biol.* **5,** e144
23. Tanaka, S., Sawaya, M. R., Phillips, M., and Yeates, T. O. (2009) *Protein Sci.* **18,** 108–120
24. Tanaka, S., Kerfeld, C. A., Sawaya, M. R., Cai, F., Heinhorst, S., Cannon, G. C., and Yeates, T. O. (2008) *Science* **319,** 1083–1086
25. Stojiljkovic, I., Bäumler, A. J., and Heffron, F. (1995) *J. Bacteriol.* **177,** 1357–1366
26. Sampson, E. M., and Bobik, T. A. (2008) *J. Bacteriol.* **190,** 2966–2971
27. Penrod, J. T., and Roth, J. R. (2006) *J. Bacteriol.* **188,** 2865–2874
28. Heinhorst, S., Williams, E. B., Cai, F., Murin, C. D., Shively, J. M., and Cannon, G. C. (2006) *J. Bacteriol.* **188,** 8087–8094
29. Dou, Z., Heinhorst, S., Williams, E. B., Murin, C. D., Shively, J. M., and Cannon, G. C. (2008) *J. Biol. Chem.* **283,** 10377–10384
30. Cheng, S., and Bobik, T. A. (2010) *J. Bacteriol.* **192,** 5071–5080
31. Otwinowski, Z., and Minor, W. (1997) *Methods Enzymol.* **276,** 307–326
32. Collaborative Computational Project, Number 4 (1994) *Acta Crystallogr. D. Biol. Crystallogr.* **50,** 760–763
33. Adams, P. D., Grosse-Kunstleve, R. W., Hung, L. W., Ioerger, T. R., McCoy, A. J., Moriarty, N. W., Read, R. J., Sacchettini, J. C., Sauter, N. K., and Terwilliger, T. C. (2002) *Acta Crystallogr. D Biol. Crystallogr.* **58,** 1948–1954
34. Bricogne, G., Blanc, E., Brandl, M., Flensburg, C., Keller, P., Paciorek, W., Roversi, P., Smart, O., Vonrhein, C., and Womack, T. (2009) *BUSTER*, Global Phasing, Ltd., Cambridge, UK
35. Tsai, Y., Sawaya, M. R., and Yeates, T. O. (2009) *Acta Crystallogr. D Biol. Crystallogr.* **65,** 980–988
36. Colovos, C., and Yeates, T. O. (1993) *Protein Sci.* **2,** 1511–1519
37. Kabsch, W. (1993) *J. Appl. Crystallogr.* **26,** 795–800
38. Sheldrick, G. M., and Schneider, T. R. (1997) *Methods Enzymol.* **277,** 319–343
39. Sheldrick, G. M. (2008) *Acta Crystallogr. A* **64,** 112–122
40. Tanaka, S., Sawaya, M. R., and Yeates, T. O. (2010) *Science* **327,** 81–84
41. Ponstingl, H., Henrick, K., and Thornton, J. M. (2000) *Proteins* **41,** 47–57
42. Parsons, J. B., Dinesh, S. D., Deery, E., Leech, H. K., Brindley, A. A., Heldt, D., Frank, S., Smales, C. M., Lünsdorf, H., Rambach, A., Gass, M. H., Bleloch, A., McClean, K. J., Munro, A. W., Rigby, S. E., Warren, M. J., and Prentice, M. B. (2008) *J. Biol. Chem.* **283,** 14366–14375
43. Crowley, C. S., Sawaya, M. R., Bobik, T. A., and Yeates, T. O. (2008) *Structure* **16,** 1324–1332
44. Klein, M. G., Zwart, P., Bagby, S. C., Cai, F., Chisholm, S. W., Heinhorst, S., Cannon, G. C., and Kerfeld, C. A. (2009) *J. Mol. Biol.* **392,** 319–333
45. Sagermann, M., Ohtaki, A., and Nikolakakis, K. (2009) *Proc. Natl. Acad. Sci. U.S.A.* **106,** 8883–8887
46. Heldt, D., Frank, S., Seyedarabi, A., Ladikis, D., Parsons, J. B., Warren, M. J., and Pickersgill, R. W. (2009) *Biochem. J.* **423,** 199–207
47. Peña, K. L., Castel, S. E., de Araujo, C., Espie, G. S., and Kimber, M. S. (2010) *Proc. Natl. Acad. Sci. U.S.A.* **107,** 2455–2460
48. Sampson, E. M., Johnson, C. L., and Bobik, T. A. (2005) *Microbiology* **151,** 1169–1177
49. Johnson, D. C., Dean, D. R., Smith, A. D., and Johnson, M. K. (2005) *Annu. Rev. Biochem.* **74,** 247–281